Non-Inductive Current Drive by EC Waves in an Inboard Poloidal Magnetic Field Null Configuration on the Spherical Tokamak QUEST*)

Saya TASHIMA[1)], Hideki ZUSHI[2)], Mitsutaka ISOBE[3)], Hiroshi IDEI[2)], Shoichi OKAMURA[3)], Kazuaki HANADA[2)], Kazuo NAKAMURA[2)], Akihide FUJISAWA[2)], Keisuke MATSUOKA[2)], Makoto HASEGAWA[2)], Yoshihiko NAGASHIMA[2)], Shoji KAWASAKI[2)], Hisatoshi NAKASHIMA[2)], Aki HIGASHIJIMA[2)] and QUEST Team

[1)]*IGSES, Kyushu University, Kasuga, Fukuoka 816-8580, Japan*
[2)]*RIAM, Kyushu University, Kasuga, Fukuoka 816-8580, Japan*
[3)]*National Institute for Fusion Science, Toki 509-5292, Japan*

(Received 21 November 2012 / Accepted 18 June 2013)

To investigate the effects of confinement of fast electrons on poloidal beta equilibrium, experiments under different toroidal magnetic mirror ratios, M_{OMFC}, were performed in electron cyclotron heated plasma in the spherical tokamak QUEST. The proportional constants of the relation between plasma current and vertical magnetic fields decreased with increase in M_{OMFC}. The poloidal field null point appeared in the chamber for $M_{\mathrm{OMFC}} > 1.8$ at a plasma current value of ~15 kA. Poloidal beta and temperature of hard X-rays increased with M_{OMFC}. This suggests that high poloidal beta equilibrium plasma is produced by better confinement of energetic trapped particles.

Keywords: non-inductive current drive, electron cyclotron resonance heating, energetic electron, high poloidal beta, trapped electron

DOI: 10.1585/pfr.8.2402118

1. Introduction

Efficient plasma current (I_{p}) startup and high performance sustainability without the use of center solenoid coils is critical for future tokamak reactors. Non-inductive current startup using electron cyclotron resonance heating (ECH) has been on several tokamaks and spherical tokamaks (STs) [1–4]. Recently, it has been suggested that I_{p} is generated by trapped particles in STs [5, 6]. To identify current drive mechanisms, the dependence of initial plasma current $I_{\mathrm{p}}^{\mathrm{initial}}$ on vertical magnetic field B_{z}, ratio of B_{z} to toloidal magnetic field (B_{t}; $B_{\mathrm{z}}/B_{\mathrm{t}}$), curvature of magnetic field lines, and decay index n^* ($= -\mathrm{d}(lnB_{\mathrm{z}})/\mathrm{d}(lnR)$) has to be examined in open magnetic fields (OMFC). In TST-2, current startup experiments have been performed using a frequency of 2.45 GHz and the B_{z} dependence of I_{p} ramp-up rate and $I_{\mathrm{p}}^{\mathrm{initial}}$ (< 1.2 kA) has been investigated under the condition of $B_{\mathrm{z}} < 1$ mT for $n^* = 0.06$ - 1.1 [4]. It has been concluded that high-energy electrons (~1 keV) play an important role on $I_{\mathrm{p}}^{\mathrm{initial}}$, but not after current ramp-up. In the QUEST device, a new startup scenario has been tested using ECWs at a high toroidal magnetic mirror ratio (M_{OMFC}) ~2 ($= n^* \sim 0.5$) with a high $B_{\mathrm{z}}/B_{\mathrm{t}}$ of 10% at the fundamental resonance layer, R_{res1} [7]. Here M_{OMFC} is defined as the ratio of B_{t} at the chamber walls (inner center stack or top/bottom plates) to B_{t} at the starting point (e.g., at second resonance layer R_{res2}) on the mid-plane along the magnetic field lines. When M_{OMFC} is increased, the width of pitch angle of trapped particles, $\Delta\theta_{\mathrm{trap}}$, in velocity space is increased. For the case of $M_{\mathrm{OMFC}} = 2$, because the field lines are strongly curved, particles whose $\Delta\theta_{\mathrm{trap}}$ is 45° - 135° can be trapped. For the case of $M_{\mathrm{OMFC}} = 1.2$, a $\Delta\theta_{\mathrm{trap}}$ value of 65° - 115° is estimated. The banana width τ_{b} relates inversely to B_{z} and proportionally with $v_{//}$. With increasing B_{z}, the banana width becomes narrower, even for high $v_{//}$. Therefore, increments of B_{z} and M_{OMFC} are favorable for confinement of energetic trapped electrons. Better confinement of energetic trapped electrons causes an increase in pressure. In these experiments [7], because of high β_{p} (ratio of plasma pressure to poloidal magnetic pressure) plasma, under high M_{OMFC} and ECW driven current, the inboard poloidal null configurations (IPNCs) characterized by high β_{p} are observed in steady state. High β_{p} plasma has been demonstrated by means of I_{p} ramp-down, NB heating, and lower hybrid current drive (LHCD) [8–10]. However, in QUEST, steady-state high β_{p} plasma bounded by the separatrix could be sustained by ECWs in high M_{OMFC} and B_{z} configurations.

In this review, we describe the manner in which confined energetic electrons contribute to p_{hot} and plasma

author's e-mail: tashima@triam.kyushu-u.ac.jp

*) This article is based on the presentation at the 22nd International Toki Conference (ITC22).

equilibrium through β_p by measuring the hard X-ray (HXR) energy spectrum. To investigate $v_\perp > v_{//}$ electrons, such as trapped electrons, the measurement of vertical line of sight (perpendicular to toroidal magnetic field lines) is conducted for different M_{OMFC} values. The relation between I_p and B_z is compared to the MHD equilibrium relation [11]:

$$B_z = \mu_0 I_p (In(8R/a) + l_i/2 - 3/2 + \beta_p)/4\pi R, \quad (1)$$

where l_i is the internal inductance. The effects of M_{OMFC} on $\beta_p = (\beta_p^{bulk} + \beta_p^{hot})$ and correlation between β_p^{hot} and HXR are investigated.

This manuscript is organized as follows. Section 2 provides a device description of the small aspect ratio chamber and experimental conditions used to sustain I_p. Section 3 discusses our investigation of the equilibrium relation of I_p - B_z for different M_{OMFC} values and energetic electron energy through measurement of HXR.

2. Experimental Setup and Conditions

QUEST is a medium-sized device, whose inner and outer diameters are 0.23 m and 1.33 m, respectively. The major (R_0) and minor ($\langle a \rangle$) radii of the plasma are 0.7 - 0.85 m and 0.2 - 0.4 m, respectively. The chamber aspect ratio A_c ($= R_c/a_c \approx 1.4$) is derived as $(R_{out} + R_{in})/(R_{in} - R_{out})$ by the chamber major radius $R_c = (R_{in} + R_{out})/2$ ($\approx$ 0.78 m) and the chamber minor radius $a_c = (R_{out} - R_{in})/2$ ($\approx$0.55 m). The chamber mirror ratio $M_{c\text{-mirror}}$ is approximated by R_c/R_{in} to be ~3.4. At $R = 0.6$ m, $M_{c\text{-mirror}}$ is 2.6. M_{OMFC} and B_z are changed by a combination of poloidal field coils and coil current value, respectively. Two flat divertor plates are set at $Z = \pm 1$ m from the mid-plane. RF waves (< 150 kW) at a frequency of 8.2 GHz are used to initiate plasma and sustain plasma current. B_t is 0.29 T at R_{res2}, and R_{res1} and R_{res2} locate at 0.3 m and 0.6 m, respectively. Two antenna systems are used; one launches ECWs at $Z = -0.08$ m in the O-mode, whose parallel refractive index is < 0.4, and another antenna system launches in the O and X mixed modes. The working gas is H_2 and is puffed 0.3 s before RF injection by a piezo valve. Typical plasma density n_e is below the cut-off density n_{cut} ($\sim 8.6 \times 10^{17}$ m^{-3}).

The measurements of energetic electrons have been performed by investigating their emitted HXR along the observation path. A semiconductor detector CdTe, with a size of 4 mm × 4 mm × 1 mm, is used to detect bremsstrahlung emitted by energetic electrons in the energy range from 10 to 500 keV, which corresponds to CdTe detector absorption efficiencies [12] of 100% to 10%, respectively. Pulse height analysis is used to obtain the energy spectrum with a time resolution of a few milliseconds. The observation lines view plasma tangentially on the mid-plane with a radial resolution of ±0.1 m at a tangential major radius of $R_{tan} = 0.6$ m. The vertical viewing chords cover the major radius on mid-plane R_{mid} from 0.2 m to 1 m with a resolution of $\Delta R_{mid} = 60$ mm (for radial scanning). The reconstruction of the flux surface is performed using 64 flux loops and a Rogowskii coil. The electron density is measured by an interferometer of 138 GHz along the horizontal path.

3. Experimental Results

To investigate how the confined energetic electrons contribute to plasma equilibrium through β_p, plasma current drive experiments under different M_{OMFC} and B_z values and measurement of HXR were conducted. M_{OMFC} was varied from 1.2 to 2 and B_z from 0.5 to 16 mT. Figure 1 shows the discharge waveforms of I_p, B_z, line integrated density $n_e l$, and HXR flux Γ_{HX} in the energy ranges of more than 50 keV.

Figure 1 a show the waveforms for the B_z ramp-up discharges under an almost constant M_{OMFC} value of ~ 1.1 - 1.2 and $P_{rf} \approx 100$ kW. To achieve $I_p \approx 15$ kA, the magnitude of B_z was temporally increased, but the inductive field was less than 10 mV. I_p increased from 5 kA at $B_z = 1.4$ mT to 15 kA at $B_z = 4$ - 5.7 mT (within 0.3 s). At $B_z \geq 4$ mT, the increase of I_p stopped. A steady application of B_z of more than 2 mT caused the termination of I_p. In steady state, the values of $n_e l \approx 2 \times 10^{17}$ m^{-3} $\Gamma_{HX} \approx 4.6 \times 10^3$ CPS were observed. Appreciable levels of Γ_{HX} started to appear at 2 s. As observed in Fig. 1 (b), B_z was

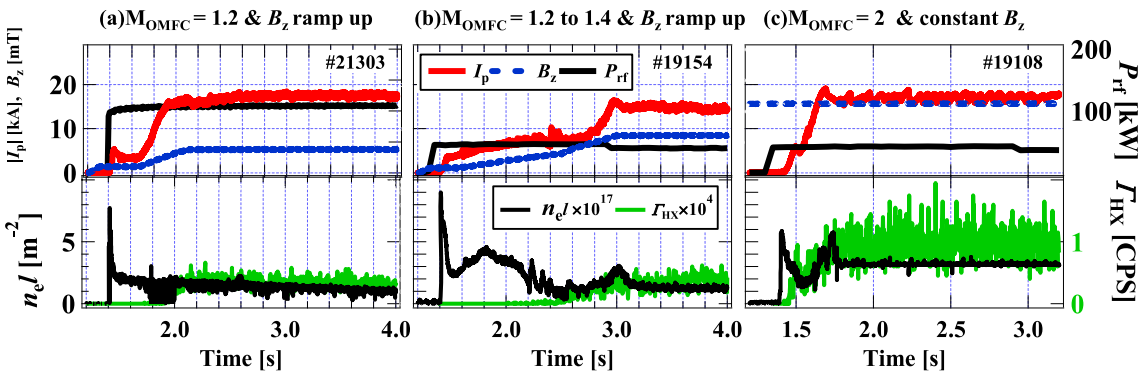

Fig. 1 Discharge wave-forms of I_p, B_z, P_{rf}, $n_e l$, and Γ_{HX} for (a) $M_{OMFC} = 1.2$, (b) $M_{OMFC} = 1.4$ (after $t = 3$ s), and (c) $M_{OMFC} = 2$.

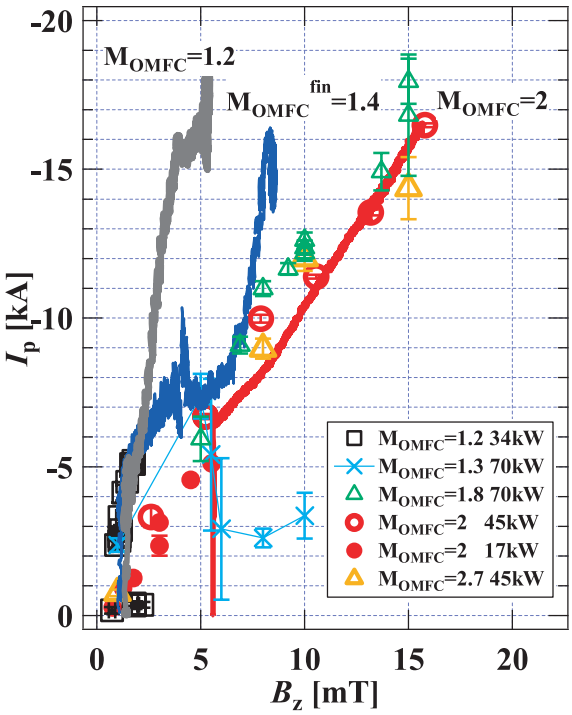

Fig. 2 I_p - B_z relation for M_{OMFC} = 1.2 (gray solid line and black squares), 1.3 (crosses), 1.4 (blue solid line), 1.8 (green triangles), 2 (red solid line, open circles, and filled circles), and 2.7 (yellow triangles). These lines and symbols correspond to B_z ramp-up discharges and constant discharges.

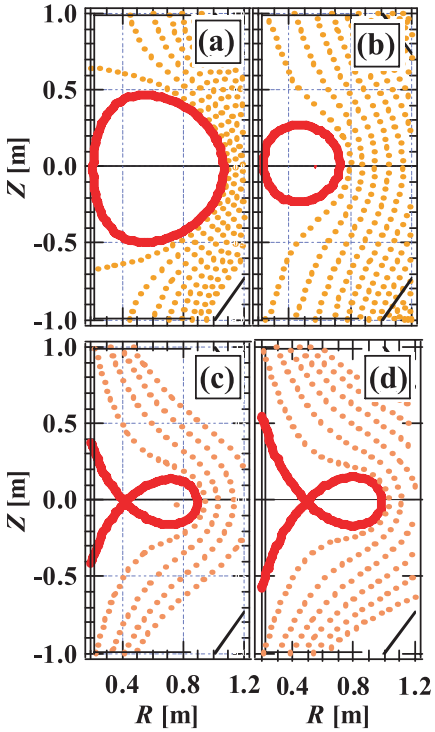

Fig. 3 Ploidal magnetic flux contours for (a) M_{OMFC} = 1.2, (b) M_{OMFC} = 1.4, (c) M_{OMFC} = 1.8, and (d) M_{OMFC} = 2.

further increased from 4 to 8 mT during the interval from 2.4 to 3.0 s and the corresponding M_{OMFC} ranges from 1.2 to 1.4 at P_{rf} = 45 kW. First, I_p was ramped up, as shown in Fig. 1 (a). Second, at t = 2.3 s, divertor and solenoid coils were switched on to increase M_{OMFC}. Finally, M_{OMFC} reached a value of 1.4. A steady state with $I_p \approx 15$ kA and $n_e l \approx 1.5 \times 10^{17}$ m^{-3} at B_z = 8 mT was obtained after t = 3 s. HXR were emitted at 2.4 s, with respect to time of start to increase M_{OMFC}, and $\Gamma_{HX} \approx 6.9 \times 10^3$ CPS was observed at steady state. Figure 1 (c) shows the discharge under constant B_z = 16 mT and M_{OMFC} = 2 at $P_{rf} \approx 45$ kW. Rapid increases of I_p (dI_p/dt = 75 kA/s) were observed, and HXR emissions began with the increases in I_p. A Γ_{HX} value of $\sim 1 \times 10^4$ CPS was observed.

To investigate the equilibrium relations between I_p and B_z, they are plotted in Fig. 2 for different M_{OMFC} values. Figure 2 shows I_p versus B_z for different M_{OMFC} values. The solid lines are the traces in the B_z - I_p space of the discharges shown in Figs. 1 (a) and (b). These lines terminated at steady state. The symbols correspond to steady state I_ps of the discharge under constant B_zs, as shown in Fig. 1 (c). For M_{OMFC} = 1.2, I_p increased linearly up to 5 kA as B_z increased to 1.7 mT, but it dropped to < 1 kA at B_z > 1.8 mT. On the other hand, at B_z ramp-up discharge, I_p reached 15 kA at 4 mT. These cases of B_z constant and ramp-up show the same proportional constant for M_{OMFC} = 1.2. For M_{OMFC} = 1.3, at constant B_z discharge (P_{rf} = 70 kW), I_p increased linearly to 7 kA as B_z increased to 5 mT and I_p decreased to 3 kA ± 0.5 kA at B_z > 6 mT. For M_{OMFC} = 1.4, I_p increased linearly up to 14 - 16 kA at B_z = 8 mT in steady state. For M_{OMFC} = 1.8, 2, and 2.7, it was not observed that I_p dropped or stopped increasing. In addition, the proportional constant of the I_p - B_z relation was maintained. For M_{OMFC} = 1.2, 1.4, and 2, the inverse of proportional constants B_z/I_p was 0.3, 0.5, and 1 mT/kA, respectively, in steady state $I_p \approx 15$ kA. This suggests that stronger B_z is required to attain the same I_p as M_{OMFC} is increased up to 2.

Figure 3 shows the reconstructed closed magnetic flux surfaces for M_{OMFC} = 1.2, 1.4, 1.8, and 2 at $I_p \approx 15$ kA ± 1 kA taken at B_z = 4.79, 8.47, and 15 mT, respectively. The first type of plasma shape (Fig. 3 (a)) is non-circular, which is characterized by an elongation κ = 1.14 (and triangularity δ = 0.24) with an aspect ratio A (= R_0 = $\langle a \rangle$ = 0.69 m/0.45 m) of 1.63 and Shafranov shift Δ = 0.047 [11]. The value of β_p is evaluated as 0.64 from Eq. (1), with an assumption of internal inductance l_i = 1.2, assumed by the parabolic profile of the plasma current. A typical low aspect ratio spherical tokamak was present. The second plasma shape is circular and small, with parameters $\langle a \rangle$ = 0.25 m, R_0 = 0.47 m, A = 1.87, κ = 1, Δ = 0.06, and β_p evaluated as 0.93. Figure 3 (c) shows an oblate shape, with parameters $\langle a \rangle$ = 0.2 m, R_0 = 0.655 m, A = 2.8, κ = 0.63, Δ = 0.124, and β_p evaluated as 3.26. Figure 3 (d) also shows the oblate shape, with parameters $\langle a \rangle$ = 0.2 m,

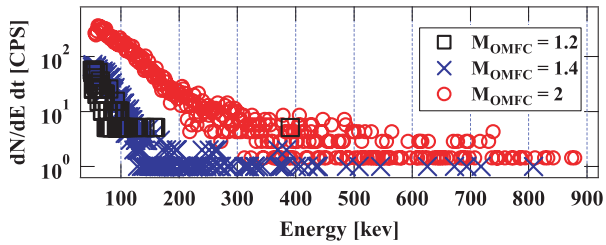

Fig. 4 Energy spectra of HXR for $M_{\mathrm{OMFC}} = 1.2$ (triangles), $M_{\mathrm{OMFC}} = 1.4$ (crosses) and $M_{\mathrm{OMFC}} = 2$ (circles).

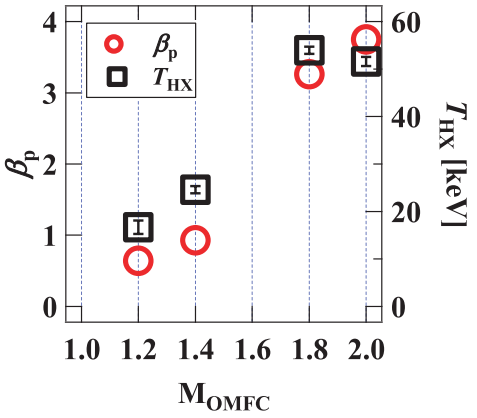

Fig. 5 β_{p} (circles) and T_{HX} (squares) as a function of M_{OMFC}.

$R_0 = 0.73$ m, $A = 2.9$, $\kappa = 0.63$, $\Delta = 0.106$, and β_{p} evaluated as 3.7. For Figs. 3 (c) and (d), the poloidal field null points appears in the chamber, which is caused by an increasing β_{p}.

Figure 4 shows the HXR energy spectra for each M_{OMFC} for $R_{\mathrm{mid}} = 0.6$ m. The energy spectra show that photon counts and energy increased with M_{OMFC}. Figure 5 shows β_{p} and HXR temperature T_{HX} as a function of M_{OMFC}. T_{HX} is calculated in the energy range of < 200 keV. Figure 5 shows that β_{p} and T_{HX} increased with M_{OMFC}. The high value of T_{HX} may be because of the rich confinement of fast electrons caused by the high M_{OMFC} and B_z configurations. Thereafter, the confined fast electrons contribute to the formation of high β_{p} plasma.

To investigate the energetic electrons on the formation of inboard poloidal null configuration accompanied by high β_{p}, a radial distribution of T_{HX} was measured. Figure 6 (a) shows the last closed flux surface of inboard poloidal null (IPN) and limiter configurations. For the limiter configuration, $I_{\mathrm{p}} \approx 15$ kA and P_{RF} was 100 kW, the same magnetic configuration as in Fig. 3 (a). I_{p} was ~10 kA and P_{RF} was 45 kW for the IPN configuration. For the IPN configuration, $\langle a \rangle = 0.15$ m, $R_0 = 0.69$ m, $A = 2.9$, $\kappa = 0.78$, $\Delta = 0.13$ m, and $\Delta/a = 0.53$. β_{p} was evaluated as 3.1 with $l_{\mathrm{i}} = 1.2$. In Fig. 6 (a), the dashed lines (blue) represent the path of HXR radial measurement. In these discharges, the HXR detection path was changed on each discharge. The shot-to-shot variation during 20 plasma discharges was monitored by another HXR detector and it was almost constant. Figure 6 (b) shows the radial profiles of T_{HX} for the limiter and IPN configurations. For the limiter configuration, the T_{HX} profiles were spatially flat and the energy was ~20 keV. For $R_{\mathrm{mid}} < 0.3$ m, because too many photons were observed, which is caused by energetic electrons being lost to inner limiter, it was impossible to calculate T_{HX}. It observed that in the IPN configuration, the photon count (80 - 300 keV) was 6 times larger than that in the limiter configuration at $R_{\mathrm{mid}} = 0.75$ m. For the IPN configuration, the T_{HX} profile peaked at $R_{\mathrm{mid}} = 0.75$ m, which corresponds to the magnetic axis. Outside of the closed flux surface, $R_{\mathrm{mid}} < 0.9$, a T_{HX} value ~25 keV was observed. The orbit analysis shows that the particles that started from $R = 0.9$ m and $Z = 0$ m were confined as trapped particles with pitch angles from 31° - 143°.

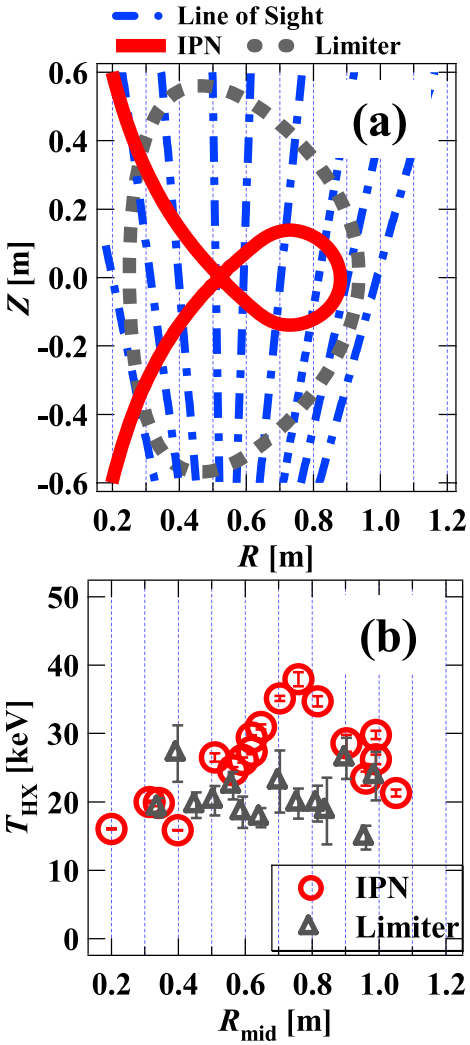

Fig. 6 (a) Last closed magnetic flux surface for limiter (dark) and IPN configurations (red). The dashed dotted lines are HXR detection paths. (b) Radial profiles of T_{HX} for the limiter (triangles) and IPN (circles) configurations.

4. Conclusion

To investigate the effects of the confinement of energetic electrons on β_p equilibrium, experiments with different confinement conditions of trapped particles were performed. We observed that with increasing M_{OMFC}, the I_p - B_z relation shows that stronger B_z is required for equilibrium at the same I_p values. Furthermore, the natural poloidal field null configuration, which is caused by high β_p, appeared as M_{OMFC} increased. The peak position of the radial profile of T_{HX} agrees fairly well with reconstructed magnetic surfaces. The role of energetic electrons on high β_p plasma was investigated by HXR, which supported the good confinement performance of energetic electrons.

Acknowledgments

It is a pleasure to acknowledge the invaluable contribution of the QUEST technical and data acquisition staffs. This work is supported by a Grant-in-aid for Scientific Research (23·4190). This work is also performed with the support and under the auspices of the NIFS Collaboration Research Program (NIFS11KUTR063).

[1] C.B. Forest *et al.*, Phys. Rev. Lett. **68**, 3559 (1992).
[2] T. Yoshinaga *et al.*, Phys. Rev. Lett. **96**, 125005 (2006).
[3] T. Maekawa *et al.*, Nucl. Fusion **45**, 1439 (2005).
[4] J. Sugiyama, A. Ejiri *et al.*, Plasma Fusion Res. **3**, 026 (2008).
[5] A. Ejiri *et al.*, Nucl. Fusion **46**, 709 (2006).
[6] T. Yoshinaga *et al.*, Plasma Fusion Res. SERIES **8**, 0100 (2009).
[7] H. Zushi *et al.*, 24th IAEA FEC EX/P2-14 (2012).
[8] G.A. Navratil *et al.*, in Plasma Phys. and Contr. Nucl. Fusion Research 1990 (Proc. 13th Int. Conf., Washington D. C., 1990), Vol. **1**, IAEA, Vienna 209 (1991).
[9] S.A. Sabbagh *et al.*, Phys. Fluids B **3**, 2277 (1991).
[10] M.E. Mauel *et al.*, Nucl. Fusion **32**, 1468 (1992).
[11] V.D. Shafranov *et al.*, *Reviews of Plasma Physics* Vol.2 (Consultants Bureau, New York, 1966).
[12] J.H. Hubbell *et al.*, Int. J. Appl. Radiat. Isot. **33**, 1269 (1982).